Check for updates

A novel approach to iron oxide separation from e-waste and bisphenol A detection in thermal paper receipts using recovered nanocomposites†

Muthumariappan Akilarasan,‡[a] Sakthivel Kogularasu,‡[a] Shen-Ming Chen, [ID] *[a] Tse-Wei Chen[a] and Bih-Show Lou*[bc]

To promote sustainability, the effective reutilization of electronic waste and profitable recovery of valuable materials from e-scrap are essential. A recent report showed that 500 million printer cartridges enter landfill annually, creating immense interest in establishing a facile recovery method for transforming waste toner into a ferrous resource. Furthermore, the European Union and US Food and Drug Administration have published guidelines concerning bisphenol A (BPA) use in the manufacture of thermal paper receipts. Accordingly, in this study, BPA levels in thermal receipts collected from various stores in Taiwan were detected by glassy carbon electrodes fabricated using graphene oxide-recovered Fe_3O_4 nanocomposites.

1. Introduction

The everyday use of electronic devices and rapid recent technological expansion have led to the production of enormous amounts of electronic waste (e-waste).[1–3] Many electronic devices, such as printers, fax machines, and photocopiers, use toner cartridges to print documents. A recent report from the "Inkjet Remanufacturers Association" stated that 1.1 billion cartridges were sold annually, with 500 million cartridges entering landfill internationally.[4–6] Those discarded cartridges contain nearly 8% of the fresh toner content, which can leak out and contaminate water sources.[7] To avoid this e-waste, we have developed a facile recovery method using magnetic separation followed by calcination to convert waste toner into an excellent ferrous resource.

Meanwhile, endocrine disruptor bisphenol A (BPA), normally used as a key component in the polythene production,[8] is hazardous to certain hormones and can adversely affect metabolism.[9–11] A recent study of the effects of BPA on pregnant women showed that even trace BPA levels can move across the placenta and damage the embryo *in utero*.[12] BPA also poses health risks such as childlessness,[13,14] damage to the central nervous system,[15,16] and behavioral variation.[17,18] Therefore,

following a prolonged study on BPA toxicity, in February 2018 the European Union and US Food and Drug Administration (FDA) publishing guidelines to prohibit BPA use as a component in thermal paper manufacture.[19–22] Accordingly, our research group collected thermal receipt paper from various stores in Taiwan, including 7-Eleven, Family Mart, PX Mart, OK Mart, Hi-Life, and KFC, as well as ATM receipts, to determine their constituent BPA levels. A standardized HPLC-UV detection method was used to detect the BPA levels in thermal receipt samples prepared using migration and digestion techniques. Surprisingly, high BPA levels were found in the collected thermal receipts. This inspired our research group to establish a trace level BPA detector. Recently, Fe_3O_4 was reported as an active participant in the selective detection of BPA,[23,24] while graphene oxide (GO) sheets have also been shown to improve the sensing capability of BPA detection.[25,26]

Herein, Fe_3O_4 nanoparticles recovered from toner were sonicated with GO nanosheets to obtain a GO–Fe_3O_4 composite, which was then fabricated onto a glassy carbon electrode (GCE). Owing to a large synergetic effect,[26] electron transfer between BPA and the electrode surface was improved by GO–Fe_3O_4, resulting in selective and stable sensing. As expected, the sensor showed superior analytical parameters against lab samples. Therefore, the prepared sensor was employed for selective and sensitive detection of BPA in real thermal receipt samples.

[a]*Department of Chemical Engineering and Biotechnology, National Taipei University of Technology, No. 1, Section 3, Chung-Hsiao East Road, Taipei 106, Taiwan. E-mail: smchen78@ms15.hinet.net; Fax: +886 2270 2523; Tel: +886 2270 17147*

[b]*Chemistry Division, Center for General Education, Chang Gung University, Taoyuan, Taiwan. E-mail: blou@mail.cgu.edu.tw; Fax: +886 3211 8700; Tel: +886 3211 8800*

[c]*Department of Nuclear Medicine and Molecular Imaging Center, Chang Gung Memorial Hospital, Taoyuan, Taiwan*

† Electronic supplementary information (ESI) available. See DOI: 10.1039/c8ra08017h

‡ These authors contributed equally.

2. Experimental

2.1 Chemicals

BPA, butyl acetate, and ethanol were purchased (see ESI, S1†) and used as received. Electrochemical studies were conducted using 0.1 M phosphate buffer (pH 7) as the supporting
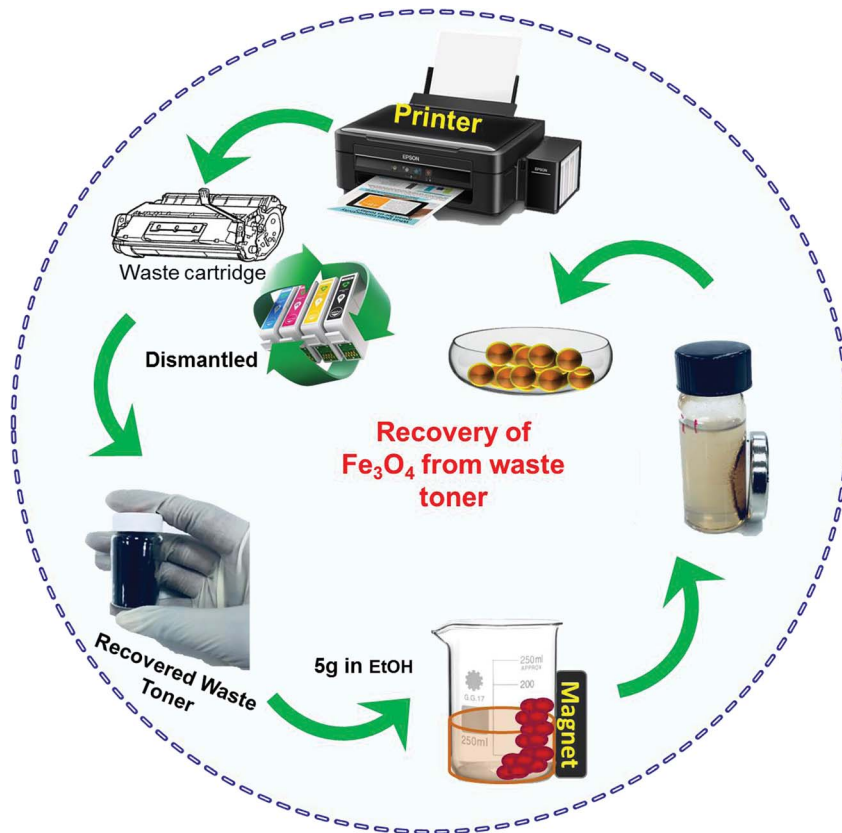
Scheme 1 Recovery procedure of Fe$_3$O$_4$ from the waste toner.

electrolyte. The preparation of electrolytes, chemical consumption, and equipment used are described in the ESI (S1†).

2.2 Extraction and purification of Fe$_3$O$_4$

Initially, discarded cartridges were dismantled to recover the waste toner inside (Scheme 1). As-obtained toner (5 g) was dissolved in ethanol (50 mL) in a beaker with a magnet attached to the side and stirred vigorously with a glass rod. When stirring was stopped, some material had settled near the magnet, while the rest remained moving in solution. The supernatant was decanted and the same stirring procedure was repeated with fresh solvent, followed by decanting again. The magnetically separated powder was collected, finely ground, dissolved in butyl acetate (15 mL), and stirred for 30 min to remove impurities inside the lumps of toner. The solution was centrifuged several times with ethanol and dried in an oven at 90 °C for 7 h. Finally, the resulting dried powder was calcined at 500 °C for 2 h. The recovered material was placed under 5% H$_2$/Ar flowing at 40 mL min^{-1} and heated from 50 °C to 500 °C at a rate of 10 °C min^{-1}. The resulting powder was further characterized.

2.3 Preparation of GO–Fe$_3$O$_4$ composite

To prepare the GO–Fe$_3$O$_4$ composite, Fe$_3$O$_4$ (1 mg) was added to GO dispersion (2 mL, 1 mg mL^{-1}) in 45% ethanol and magnetically stirred for 15 min. The resulting mixture was ultrasonicated for another 15 min, which ensured sufficient interfacial self-assembly of negative GO sheets on positively charged Fe$_3$O$_4$ *via* electrostatic interactions, resulting in a stable network of Fe$_3$O$_4$ encapsulated by thin layers of GO.

3. Results and discussion

3.1 Structural and elemental characterization

Morphological and structural information for the recovered Fe$_3$O$_4$, graphene oxide, and GO–Fe$_3$O$_4$ composite were obtained using FE-SEM. The size of recovered Fe$_3$O$_4$ was determined using the particle size distribution plot (Fig. S4†) and scaled to a mean size of 109 nm, as shown in Fig. 1A. Fig. 1B shows the thin GO sheets. Our previously reported procedure was used to prepare GO,[27] which was then ultrasonicated with the recovered Fe$_3$O$_4$ nanoparticles to obtain the composite, as shown in Fig. 1C and D, with different magnifications. The fine thin GO sheets enveloped each of the recovered spheres, as also confirmed using TEM (Fig. 2A and B). Elemental detection of the recovered ferrous material was conducted to determine the presence of impurities, as detailed in the ESI (S2†).

Fig. 3A shows the survey spectrum of the GO–Fe$_3$O$_4$ composite. Characteristic O 1s, C 1s, Fe 2p, and Fe 3p peaks were identified. The drastic increase in the O 1s and C 1s intensities was due to the presence of graphene oxide, which covered the surface of recovered Fe$_3$O$_4$. Fig. 3B shows the Fe 2p spectrum of GO–Fe$_3$O$_4$, in which the peaks at 710.2 and 724.9 eV
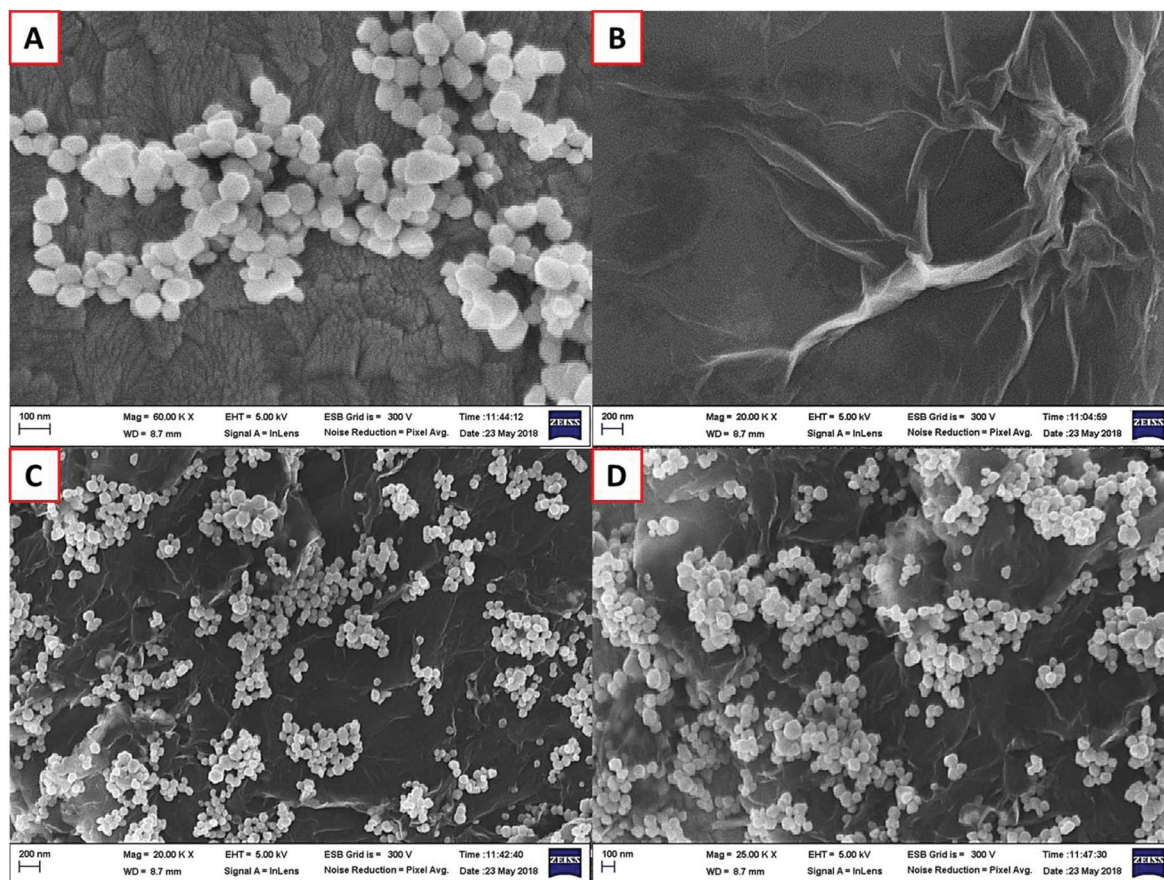
Fig. 1 FE–SEM images of Fe_3O_4 (A) and GO (B), and GO–Fe_3O_4 (C and D).

are assigned to Fe $2p_{3/2}$ and Fe $2p_{1/2}$, respectively, which confirmed that the particles recovered from waste toner were Fe_3O_4 nanoparticles.[28] The small peak at 720 eV, found between those of Fe $2p_{3/2}$ and Fe $2p_{1/2}$, indicated the presence of smaller amounts of Fe_2O_3.[28] The inset of Fig. 3B shows that the Fe $2p_{3/2}$ peak was well fitted with two deconvoluted peaks at around

712 eV and 710 eV, which were attributed to Fe^{3+} (major) and Fe^{2+} (minor), respectively.[29] Therefore, the presence of Fe_3O_4 was confirmed by XPS analysis.

The XRD pattern of recovered Fe_3O_4 nanoparticles is shown in Fig. S3,† which shows the characters of Fe_3O_4 nanoparticles with distinct crystallinity. Overall, the diffraction peaks
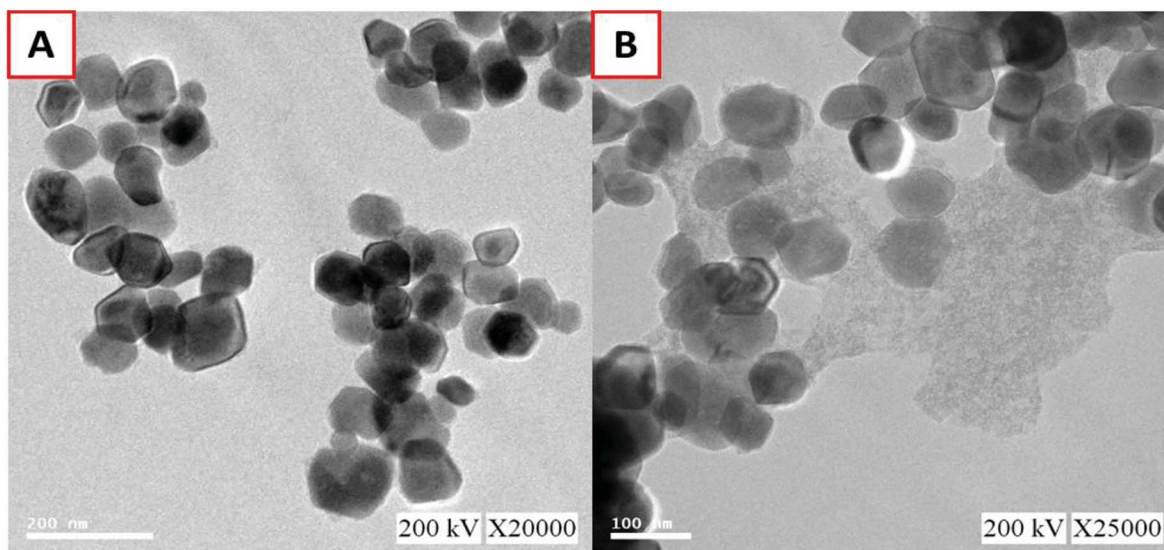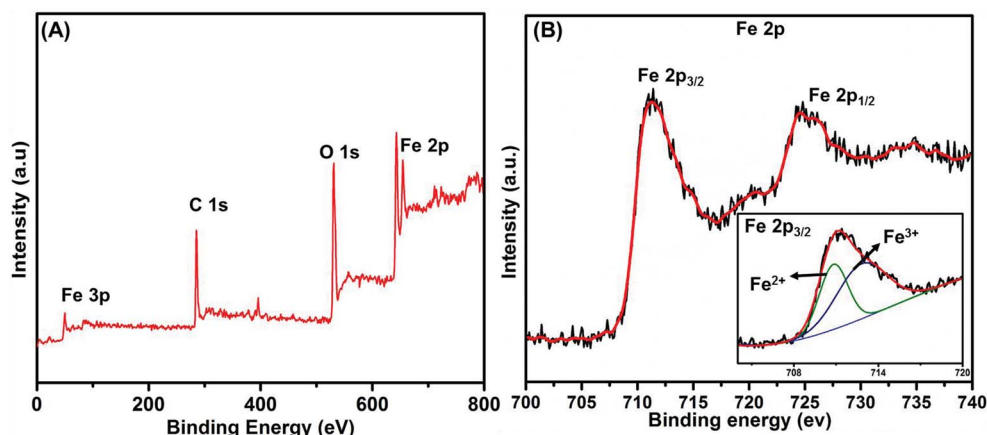

Fig. 2 TEM images of Fe_3O_4 (A) and GO-Fe_3O_4 (B).

Fig. 3 (A) Survey spectrum of Fe_3O_4/GO, and (B) high-resolution spectrum of Fe 2p (inset: deconvoluted peaks of Fe $2p_{3/2}$).

correlated well with characteristic peaks of the Fe_3O_4 inverse spinel structure (PCPDFWIN v.2.02, PDF no. 89-0691). No obvious impurity peaks were found in the diffraction pattern.

Fig. 4A and B show the BET surface analysis of Fe_3O_4 and $GO-Fe_3O_4$. Both materials had type 1 isotherms. The BET surface areas were found to be 4.3924 m^2 g^{-1} for Fe_3O_4 nanoparticles and 25.2086 m^2 g^{-1} for $GO-Fe_3O_4$.

3.2 Electrocatalytic properties of Fe_3O_4- and $GO-Fe_3O_4$-modified GCEs

The electrochemical kinetics of different electrodes were investigated using the ($[Fe(CN)_6]^{3-/4-}$) redox probe. Fig. 5A shows the CVs of unmodified GCE, GO/GCE, Fe_3O_4/GCE, and Fe_3O_4/GO/GCE containing 0.05 M of $[Fe(CN)6]^{3-/4-}$ at a scan rate of 0.05 V s^{-1}. Compared with the other modified electrodes Fe_3O_4/GO/GCE showed an excellent redox peak, good electrochemical conductivity, and tolerable peak-to-peak potential separation (ΔE_p). The calculated ΔE_p values of bare GCE, GO/GCE, Fe_3O_4/GCE, and Fe_3O_4/GO/GCE were 145, 123, 84, and 52 mV, respectively. The cathodic to anodic peak current ratio (I_{p_c}/I_{p_a}) of Fe_3O_4/GO/GCE was 0.98, which is close to 1, confirming that the reaction is reversible. Furthermore, the I_{p_c}/I_{p_a}

ratios of unmodified GCE, GO/GCE, and Fe_3O_4/GCE were 0.91, 0.93, and 0.95, respectively. The electroactive surface area (EASA) of the recovered material and its composites were measured using the Randles–Sevcik equation (eqn (1)).[30,31] Meanwhile, by altering the scan rates, the kinetics in the $[Fe(CN)_6]^{3-/4-}$ system were investigated (Fig. 5B).

$$I_p = 2.69 \times 10^5 n^{3/2} A D^{1/2} C v^{1/2} \qquad (1)$$

The EASA values of bare GCE, GO/GCE, Fe_3O_4/GCE, and Fe_3O_4/GO/GCE were calculated as 0.082, 0.119, 0.166, and 0.193 cm^2, respectively, from the slope of I_{p_a} vs. $v^{1/2}$. Furthermore, CV studies observed at different scan rates elucidated the pseudo-capacity of Fe_3O_4/GO/GCE. The greater charge diffusion polarization of the recovered Fe_3O_4/GO/GCE was indicated by the increased peak current.

3.3 Voltammetric response of modified electrodes towards BPA

The electrochemical sensing behavior of different modified electrodes towards BPA oxidation was evaluated in 0.1 M
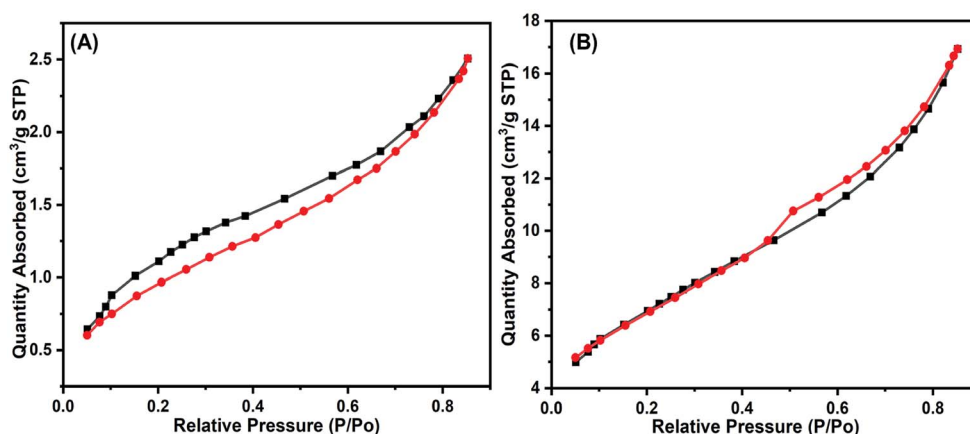

Fig. 4 BET surface analysis of Fe_3O_4 (A) and $GO-Fe_3O_4$ (B).

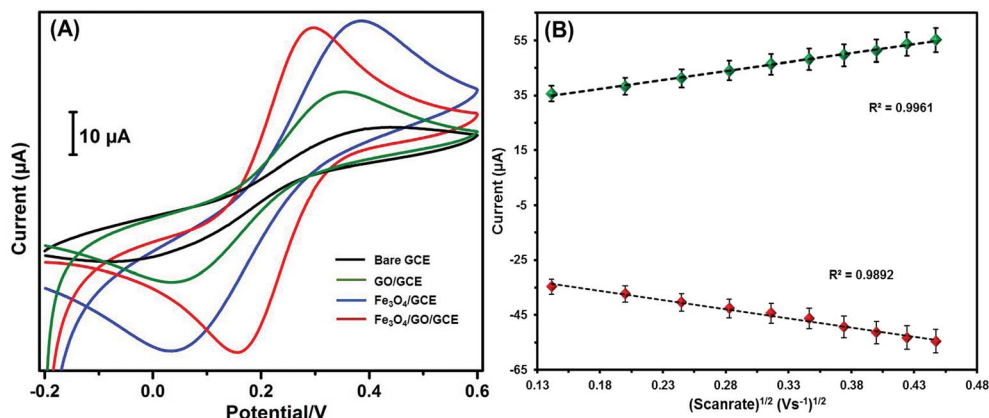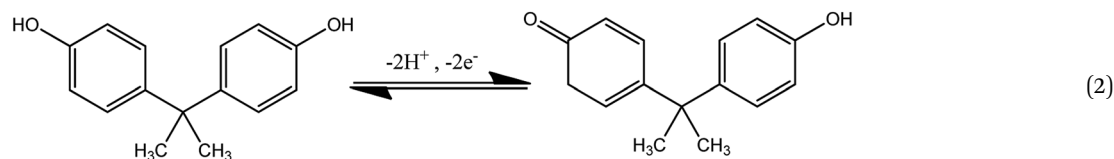**Fig. 5** (A) CVs of bare GCE, GO/GCE, Fe_3O_4/GCE and Fe_3O_4/GO/GCE in 0.1 M KCl containing 5 mM $[Fe(CN)_6]^{3-/4-}$, and (B) Fe_3O_4/GO/GCE calibration plot of I_{p_c}/I_{p_a} vs. $v^{1/2}$.

phosphate buffer solution (PBS) at a scan rate of 0.05 V s^{-1}. Fig. 6A shows the CVs of bare GCE, GO/GCE, Fe_3O_4/GCE, and Fe_3O_4/GO/GCE with BPA (50 μM) in 0.1 M PBS. No oxidation peak current was observed for the unmodified GCE. Furthermore, the oxidation peak current value observed for Fe_3O_4/GO/GCE was notable among the other modified electrodes. This confirmed that the Fe_3O_4/GO/GCE modified electrode had a higher peak current response and more capable active electron transmission movement than the other modified electrodes. A possible electrochemical oxidation mechanism of BPA is shown in eqn (2).

3.5 Electrochemical performance of Fe_3O_4/GO/GCE towards BPA

Fig. 6C shows the CVs of Fe_3O_4/GO/GCE obtained with increasing BPA concentration (10–100 μM) at a scan rate of 0.05 V s^{-1} in 0.1 M PBS. The outstanding oxidation peak current intensified with increasing BPA concentration. The linear plot of oxidation peak current vs. BPA concentration is shown in Fig. 6D. The linear regression equation was calculated to be I_{p_a} (μA) $= 0.2278 - 0.3567c$ (μM), $R^2 = 0.9964$.

$$\text{HO}\text{—}\bigcirc\text{—}\overset{CH_3}{\underset{CH_3}{C}}\text{—}\bigcirc\text{—OH} \xrightarrow[\ ]{-2H^+, -2e^-} \text{O}=\bigcirc\text{—}\overset{CH_3}{\underset{CH_3}{C}}\text{—}\bigcirc\text{—OH} \qquad (2)$$

3.4 Effect of pH on Fe_3O_4/GO/GCE

To determine the ideal pH for BPA detection by Fe_3O_4/GO/GCE, the electrochemical oxidation of BPA was conducted in different buffer solutions (pH 3–11) and the changes in oxidation peak current with changing pH were plotted. Fig. 6B-blue shows the graphical plot for pH vs. obtained current, evidently showing the most intense oxidation peak current at pH 7. The linearity of BPA detection was confirmed by the peak potential (E_p) plot, as shown in Fig. 6B-green. The acquired slope value for BPA (−53.2 mV) was near to the value mentioned in the Nernst equation,[32] which confirmed that the same number of protons and electrons were involved in the reduction mechanism on Fe_3O_4/GO/GCE.

CVs were recorded for Fe_3O_4/GO/GCE in 0.1 M PBS containing BPA (50 μM) at different scan rates (20–200 mV s^{-1}), as shown in Fig. 6E. Increasing the scan rate resulted in a linear increase in the anodic and cathodic peak currents. The calibration plot of the square root of scan rate vs. oxidation peak current is shown in Fig. 6F. The linear regression equation was calculated as I_{p_a} (μA) $= 38.838 + 3.7743$ and the correlation coefficient was 0.9982, indicating that the reaction was a surface-confined process.

3.6 Amperometric detection of BPA

To define the analytical efficacy of GO–Fe_3O_4, amperometric-it was executed for BPA detection. As shown in Fig. 7A, as the BPA concentration was increased from 0.025 μM to 100 μM, the oxidation peak current increased linearly without any larger

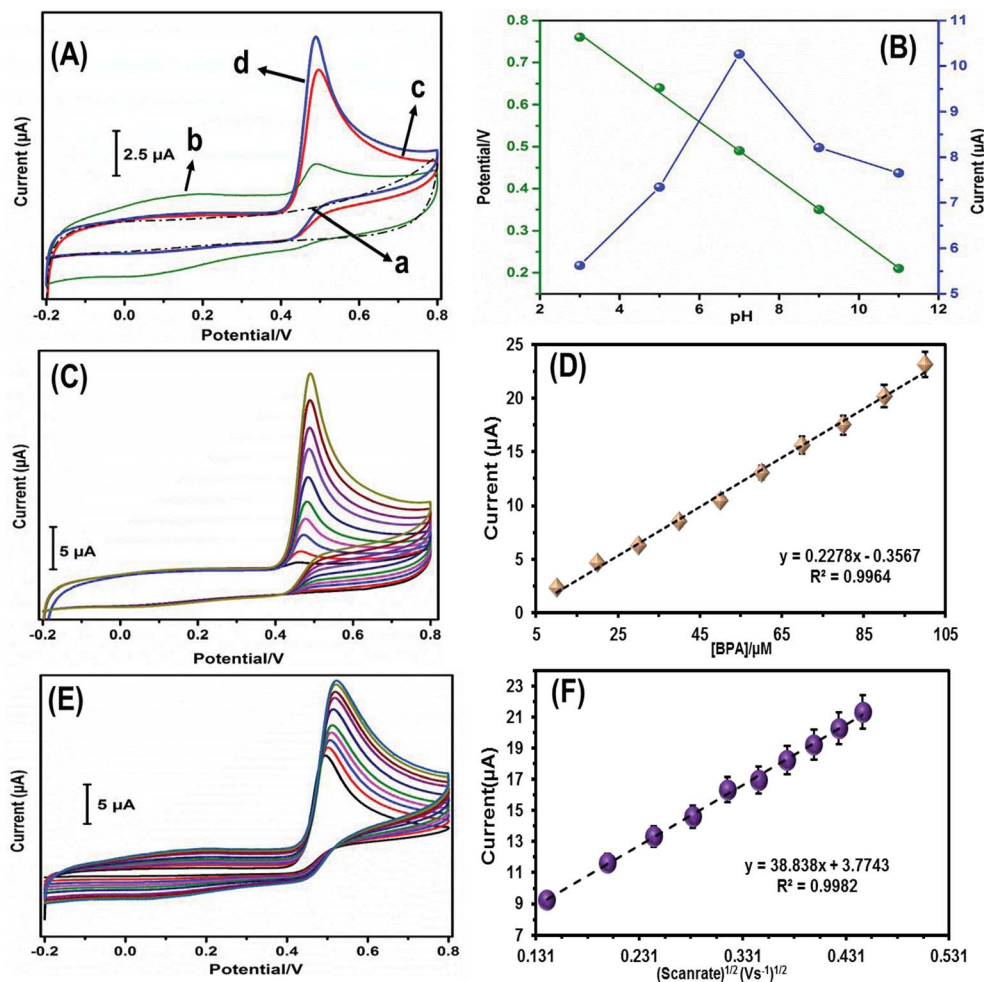**Fig. 6** (A) CVs of bare GCE (a), GO/GCE (b), Fe_3O_4/GCE (c), and Fe_3O_4/GO/GCE (d) in 0.1 M pH 7 containing 50 μM of BPA. (B) The plot of different pH $vs.$ potential (green) and different pH $vs.$ current (blue) containing 50 μM of BPA. (C) CVs obtained at Fe_3O_4/GO/GCE containing BPA (10 μM to 100 μM) in 0.1 M pH 7. (D) Calibration plot of [BPA]/μM $vs.$ current (μA). (E) CVs obtained at Fe_3O_4/GO/GCE in 0.1 M pH 7 containing 50 μM of BPA at different scan rates (20 to 200 mV s^{-1}). (F) (Scan rate)$^{1/2}$ (V s^{-1})$^{1/2}$ $vs.$ peak currents (μA).

vacillations (Fig. 7B). Therefore, GO–Fe_3O_4 was suitable for the trace level detection of BPA. This yielded a wider linear range of 25 nM to 782.75 μM, with a very low detection limit of 6.9 nM. The sensitivity towards BPA was calculated as 2.62238 μA μM^{-1} cm^{-2}. Therefore, GO–Fe_3O_4 has superior parameters, which are necessary for an effective sensor. Finally, the linear range and LOD were compared with previously reported BPA sensors (Table 1), with the GO–Fe_3O_4 modified electrode showing excellent sensing properties toward BPA detection. As a control study, GO was fabricated onto a GCE instead of GO–Fe_3O_4, and the amperometric study was performed. The results obtained for GO were compared with those of GO–Fe_3O_4, as shown in Fig. S6A.† Fig. S6B† shows the linear plot of the pure GO modified electrode, with the linear range and limit of detection were calculated as 1–559 μM and 821.2 nM, respectively.

3.7 BPA selectivity

The BPA selectivity was measured using an amperometric technique in 0.1 M PBS. To determine the selectivity of the GO–

Fe_3O_4 adapted electrode, interfering substances (200 μM) were added in the presence of BPA (50 μM), as shown in Fig. 7C. As a result, the interfering components showed a negligible current response and indicated satisfactory selectivity for BPA sensing.

3.8 Repeatability, reproducibility, and durability

The reusability of the prepared electrode was examined over ten uses in 0.1 M PBS containing BPA (50 μM) at 50 mV s^{-1}, with the corresponding current responses plotted. After using ten times, the electrode showed 98.2% of its initial current response, indicating that Fe_3O_4/GO/GCE has excellent reusability. In addition to investigating the repeatability, different Fe_3O_4/GO/GCE samples were freshly prepared and their CV responses recorded and response currents plotted, as shown in the ESI (S5†). The RSD was calculated as 3.17%, which indicated that Fe_3O_4/GO/GCE had excellent repeatability in BPA sensing. Furthermore, the sensor stability was monitored daily (Fig. 7D). After continuous use for 15 days, the sensor maintained 97.95%
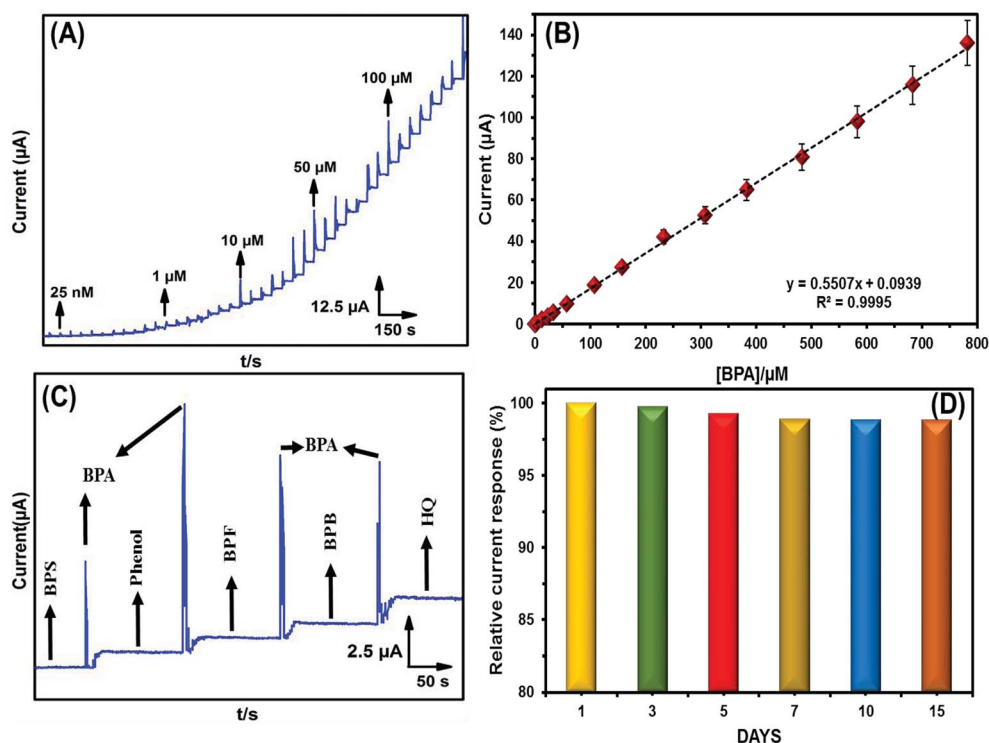
Fig. 7 (A) Amperometric response of Fe_3O_4/GO modified electrode for each sequential additions of BPA into 0.1 pH 7, the rotation speed = 1200 rpm. (B) The plot of [BPA]/μM *vs.* current (μA). E_{app} = 0.46 V (*vs.* Ag/AgCl). (C) Amperometric selective responses of Fe_3O_4–GO towards 50 μM of BPA. (D) Stability of the sensor as its continuous usage of 15 days.

Table 1 Comparison of analytical parameters obtained for GO–Fe_3O_4 film-modified electrode toward BPA with previous reports

Electrode	LOD (nM)	Linear range (μM)	Method	Reference
[a]GN film electrode	35	0.1–100	DPV	33
[b]CS/[c]MNPs-[d]rGO/[e]GCE	16.7	0.06–11	DPV	26
[b]CS-Fe_3O_4/[d]GCE	8	0.05–30	DPV	23
[f]MWCNTs/[g]PCV/[e]GCE	10	0.05–100	LSV	34
[d]rGO-Ag/[h]PLL	540	1–80	DPV	35
Cu_2O-[d]rGO	53	0.1–80	AMP	36
Fe_3O_4/GO/GCE	6.9	0.025–782.75	AMP	This work

[a] GN, graphite nanoparticles. [b] CS, chitosan. [c] MNPs, magnetic nanoparticles. [d] rGO, reduced graphene oxide. [e] GCE, glassy carbon electrode. [f] MWCNT, multi-walled carbon nanotubes. [g] PCV, poly crystal violet. [h] PLL, poly-L-lysine.

of its initial response. From these results, $Fe_3O_4/GO/GCE$ showed superior efficacy toward BPA sensing.

3.9 Real sample investigation

The practicality of the equipped sensor was tested on thermal receipt samples collected from the various convenience stores, restaurants, and ATMs in Taiwan. The sample preparation procedures are explained under their classifications in Scheme 2. The BPA concentration levels found in the thermal receipts are shown in Table 2. A standardized HPLC-UV method was first

used to detect the BPA levels in thermal receipts, then the developed sensor, $Fe_3O_4/GO/GCE$, was used to detect BPA in the same samples. Finally, the results obtained by the developed electrode were compared with those of the standardized method (HPLC-UV). The found and recovered contents of the real samples are shown in Table 3. The "Added" category in Table 3 denotes the BPA levels in the thermal receipts confirmed by HPLC.

3.10 Migration technique

For the migration technique, the sample was prepared as follows. Initially, each thermal receipts was gently rubbed with a separate kimwipe lightly dampened with methanol. These kimwipes were placed in corresponding vials containing methanol (20 mL). After 2 h, the solution was collected, filtered through a nylon filter, and transferred into a sample vial. Finally, the solution was taken for HPLC analysis. For the comparison study, the same samples were subjected to the amperometric technique.

3.11 Digestion technique

Samples for digestion analysis were prepared by cutting the thermal receipts into small pieces and placing these pieces in separate vials containing methanol (20 mL). The samples were left undisturbed for 2 h, then filtered through the nylon filter, and transferred into sample vials. The final solutions were subjected to HPLC and amperometric analyses.
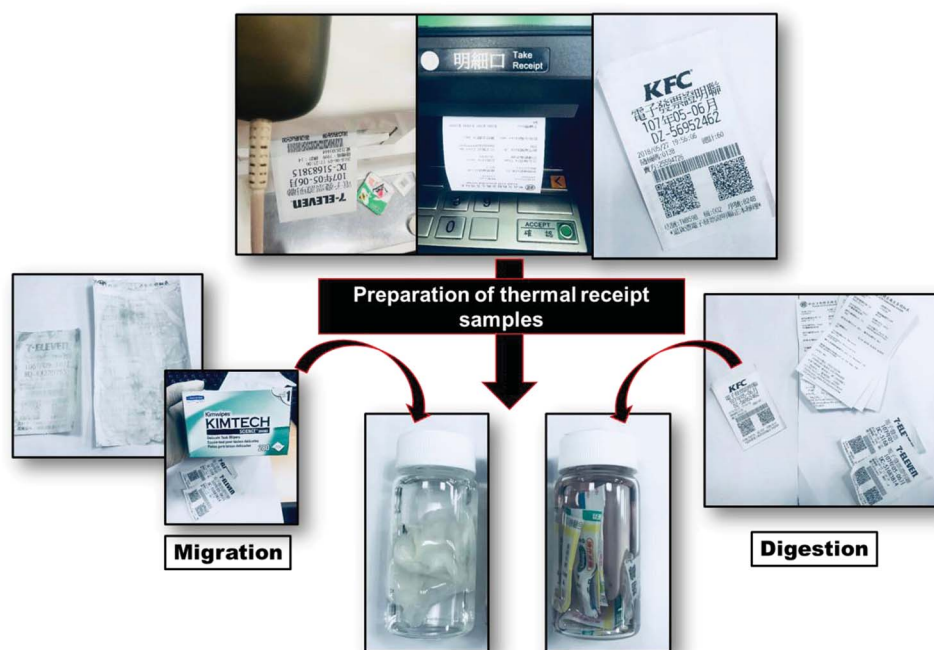
Scheme 2 Preparation procedure of thermal receipt samples.

Table 2 BPA[a]

	HPLC-UV	
Thermal receipts	Migration (ng mL^{-1})	Digestion (ng mL^{-1})
Convenience store-1	4.52	6.26
Convenience store-2	5.96	7.5
Convenience store-3	5.02	6.49
Restaurant-1	12.09	14.56
Restaurant-2	9.25	11.62
Restaurant-3	10.36	12.41
ATM receipts	ND	ND

[a] Concentration levels in thermal receipts.

Table 3 Comparison of BPA detection in thermal receipts using the developed Fe$_3$O$_4$/GO/GCE (found) and an HPLC method (added)

Thermal receipts	Added (μM)	Found (μM)	Relative error (%)	[a]RSD (%)	Average recovery (%)
Convenience store-1	0.0198	0.0191	3.53	3.97	96.44
Convenience store-2	0.022	0.0215	2.72	3.42	97.72
Convenience store-3	0.028	0.0269	3.92	4.11	96.07
Restaurant-1	0.063	0.0619	1.07	3.19	98.25
Restaurant-2	0.05	0.0484	4.02	2.63	96.8
Restaurant-3	0.054	0.0529	2.03	3.51	97.96

[a] Related standard deviation of three independent experiments.

4. Conclusions

In brief, Fe$_3$O$_4$ nanoparticles were prepared from waste toner by magnetic separation and thermal treatment. The recovered Fe$_3$O$_4$ nanoparticles were sonicated with graphene oxide nanosheets to obtain a GO–Fe$_3$O$_4$ composite. The structural, morphological, and electrochemical properties of the prepared nanocomposite were confirmed using FE-SEM, XPS, EDX, and

voltammetric analysis. The recovered material was then fabricated onto a glassy carbon electrode and evaluated for BPA sensing, exhibiting outstanding electrocatalytic properties. As a BPA sensor, GO–Fe_3O_4 exhibited a very low detection limit of 6.9 nM with a wider linear range of 25 nM to 782.75 μM. This beneficial and reliable methodology for Fe_3O_4 recovery could be effective and economic for wide-scale ferrous production, and used in sensor development for the detection of hazardous BPA in thermal receipts.

Conflicts of interest

The authors declare no conflicts of interest.

Acknowledgements

References

1 J. Cui and L. Zhang, *J. Hazard. Mater.*, 2008, **158**, 228–256.
2 R. Widmer, H. Oswald-Krapf, D. Sinha-Khetriwal, M. Schnellmann and H. Böni, *Environ. Impact Assess. Rev.*, 2005, **25**, 436–458.
3 B. H. Robinson, *Sci. Total Environ.*, 2009, **408**, 183–191.
4 E. Sundin and H. M. Lee, in *Design for innovative value towards a sustainable society*, Springer, 2012, pp. 552–557.
5 H.-Y. Kang, Y.-S. Jun, Y.-C. Kim and H.-J. Jo, *Procedia CIRP*, 2016, **40**, 280–284.
6 V. Gaikwad, U. Kumar, F. Pahlevani, A. Piadasa and V. Sahajwalla, *ACS Sustainable Chem. Eng.*, 2017, **5**, 11543–11550.
7 D. Wang, Z. Cai, G. Jiang, A. Leung, M. H. Wong and W. K. Wong, *Chemosphere*, 2005, **60**, 810–816.
8 T. Yamamoto and A. Yasuhara, *Chemosphere*, 1999, **38**, 2569–2576.
9 K. Moriyama, T. Tagami, T. Akamizu, T. Usui, M. Saijo, N. Kanamoto, Y. Hataya, A. Shimatsu, H. Kuzuya and K. Nakao, *J. Clin. Endocrinol. Metab.*, 2002, **87**, 5185–5190.
10 R. T. Zoeller, R. Bansal and C. Parris, *Endocrinology*, 2005, **146**, 607–612.
11 W. Zhou, J. Liu, L. Liao, S. Han and J. Liu, *Mol. Cell. Endocrinol.*, 2008, **283**, 12–18.
12 R. P. Sharma, M. Schuhmacher and V. Kumar, *Sci. Total Environ.*, 2018, **624**, 55–68.
13 F. S. Vom Saal, P. S. Cooke, D. L. Buchanan, P. Palanza, K. A. Thayer, S. C. Nagel, S. Parmigiani and W. V. Welshons, *Toxicol. Ind. Health*, 1998, **14**, 239–260.
14 K. L. Howdeshell, A. K. Hotchkiss, K. A. Thayer, J. G. Vandenbergh and F. S. Vom Saal, *Nature*, 1999, **401**, 763.
15 M. Aydoğan, A. Korkmaz, N. Barlas and D. Kolankaya, *Toxicology*, 2008, **249**, 35–39.
16 H. Kabuto, M. Amakawa and T. Shishibori, *J. Life Sci.*, 2004, **74**, 2931–2940.
17 M. Kundakovic, K. Gudsnuk, B. Franks, J. Madrid, R. L. Miller, F. P. Perera and F. A. Champagne, *Proc. Natl. Acad. Sci. U. S. A.*, 2013, **110**, 9956–9961.
18 J. T. Wolstenholme, M. Edwards, S. R. Shetty, J. D. Gatewood, J. A. Taylor, E. F. Rissman and J. J. Connelly, *Endocrinology*, 2012, **153**, 3828–3838.
19 C. Liao, F. Liu and K. Kannan, *Environ. Sci. Technol.*, 2012, **46**, 6515–6522.
20 S. Biedermann, P. Tschudin and K. Grob, *Anal. Bioanal. Chem.*, 2010, **398**, 571–576.
21 C. Liao and K. Kannan, *Environ. Sci. Technol.*, 2011, **45**, 9372–9379.
22 E. Union, *Official Journal of the European Union*, 2009, **5**, 2009.
23 C. Yu, L. Gou, X. Zhou, N. Bao and H. Gu, *Electrochim. Acta*, 2011, **56**, 9056–9063.
24 M. A. Subhan, P. C. Saha, M. Alam, A. M. Asiri, M. Al-Mamun and M. M. Rahman, *J. Environ. Chem. Eng.*, 2018, **6**, 1396–1403.
25 H. Fan, Y. Li, D. Wu, H. Ma, K. Mao, D. Fan, B. Du, H. Li and Q. Wei, *Anal. Chim. Acta*, 2012, **711**, 24–28.
26 Y. Zhang, Y. Cheng, Y. Zhou, B. Li, W. Gu, X. Shi and Y. Xian, *Talanta*, 2013, **107**, 211–218.
27 S. Kogularasu, M. Govindasamy, S.-M. Chen, M. Akilarasan and V. Mani, *Sens. Actuators, B*, 2017, **253**, 773–783.
28 S. Saha, M. Jana, P. Samanta, N. C. Murmu, N. H. Kim, T. Kuila and J. H. Lee, *RSC Adv.*, 2014, **4**, 44777–44785.
29 F. Han, L. Ma, Q. Sun, C. Lei and A. Lu, *Nano Res.*, 2014, **7**, 1706–1717.
30 K. Ngamchuea, S. Eloul, K. Tschulik and R. G. Compton, *J. Solid State Electrochem.*, 2014, **18**, 3251–3257.
31 X. Wang, A. Sumboja, M. Lin, J. Yan and P. S. Lee, *Nanoscale*, 2012, **4**, 7266–7272.
32 M. M. Walczak, D. A. Dryer, D. D. Jacobson, M. G. Foss and N. T. Flynn, *J. Chem. Educ.*, 1997, **74**, 1195.
33 X. Dong, X. Qi, N. Liu, Y. Yang and Y. Piao, *Sensors*, 2017, **17**, 836.
34 W. Wang, J. Tang, S. Zheng, X. Ma, J. Zhu, F. Li and J. Wang, *Food Anal. Methods*, 2017, **10**, 3815–3824.
35 Y. Li, H. Wang, B. Yan and H. Zhang, *J. Electroanal. Chem.*, 2017, **805**, 39–46.
36 R. Shi, J. Liang, Z. Zhao, A. Liu and Y. Tian, *Talanta*, 2017, **169**, 37–43.